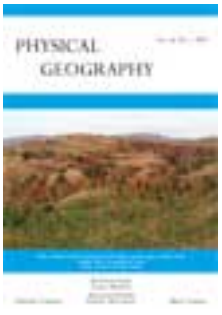

Physical Geography
Publication details, including instructions for authors and subscription information:
http://www.tandfonline.com/loi/tphy20

Quantifying successional land cover after clearing of tropical rainforest along forest frontiers in the Congo Basin

Tom Akkermans[a], Anton Van Rompaey[a], Nicole Van Lipzig[a], Pieter Moonen[b] & Bruno Verbist[b]

[a] Department of Earth and Environmental Sciences, Division of Geography, Katholieke Universiteit Leuven, Leuven, Belgium

[b] Department of Earth and Environmental Sciences, Division of Forest, Nature and Landscape, Katholieke Universiteit Leuven, Leuven, Belgium

Published online: 07 Nov 2013.

To cite this article: Tom Akkermans, Anton Van Rompaey, Nicole Van Lipzig, Pieter Moonen & Bruno Verbist , Physical Geography (2013): Quantifying successional land cover after clearing of tropical rainforest along forest frontiers in the Congo Basin, Physical Geography

To link to this article: http://dx.doi.org/10.1080/02723646.2013.855698

Physical Geography, 2013
http://dx.doi.org/10.1080/02723646.2013.855698

Taylor & Francis
Taylor & Francis Group

Quantifying successional land cover after clearing of tropical rainforest along forest frontiers in the Congo Basin

Tom Akkermans[a]*, Anton Van Rompaey[a], Nicole Van Lipzig[a], Pieter Moonen[b] and Bruno Verbist[b]

[a]*Department of Earth and Environmental Sciences, Division of Geography, Katholieke Universiteit Leuven, Leuven, Belgium;* [b]*Department of Earth and Environmental Sciences, Division of Forest, Nature and Landscape, Katholieke Universiteit Leuven, Leuven, Belgium*

(*Received 26 January 2013; accepted 26 September 2013*)

State-of-the-art impact-modeling studies in environmental and climatological sciences require detailed future deforestation scenarios that allow forest to be replaced by a mosaic of multiple successional land-cover types, rather than the simple conversion of forest to a single land-cover type, such as bare soil or cropland. Therefore, not only the amount and location of forest removal has to be known (as is typically provided by scenarios), but also knowledge about the successional land-cover types and their relative areal proportions is needed. The main objective of this study was to identify these successional land-cover types and quantify their areal proportions in regions deforested during the past 37 years around the city of Kisangani, D.R. Congo. The fallow vegetation continuum was categorized in different stages, adapted from existing classifications. Ground-truth points describing the present-day vegetation were obtained during a field campaign and used for supervised and validated land-cover classification of these categories, using the Landsat image of 2012. Areal proportions of successional land-cover types were then derived from the resulting land-cover map. The second objective of this study was to relate these areal proportions to time since deforestation, which is expected to influence fallow landscapes. Landsat images of 1975, 1990, and 2001 were analyzed. Present-day mature tree fallow is less abundant on areas deforested during 1975–1990. The relative areal proportions were used to refine a deforestation scenario and apply it to existing data-sets of LAI and canopy height (CH). Assuming a simple conversion of forest to cropland, the deforestation scenario projected a reduction of grid-cell-averaged CH from 25.5 to 7.5 m (within deforested cells), whereas the refined scenarios that we propose show more subtle changes, with a reduced CH of 13 m. This illustrates the importance of taking successional land cover correctly into account in environmental and climatological modeling studies.

Keywords: successional land cover; GIS; land cover change; Central Africa; fallow cycle

1. Introduction and problem statement

Future deforestation scenarios are essential for impact-modeling studies in environmental (e.g., biodiversity) and climatological (e.g., carbon stocks, land-atmosphere fluxes) sciences. For many studies investigating the impact of deforestation on the regional climate, the uncertainty of the results is often related to the implemented deforestation

*Corresponding author. Email: tom.akkermans@ees.kuleuven.be

scenario. The first climatologically applied deforestation scenarios consisted of a mass removal of all rainforest, replaced it either with bare soil (BS), crops or grassland, and involved a horizontal resolution of 100–300 km (Polcher & Laval, 1994; Semazzi & Song, 2001; Sud et al., 1996). Over time, a more detailed approach was adopted by implementing existing future land-cover projections, such as IMAGE (Strengers, Leemans, Eickhout, Vries, & Bouwman, 2004). These still relatively coarse-resolution projections (around 50 km), usually predict for the next 50 years, contain spatially explicit processes of fragmented desertification and deforestation, and have frequently been used in climatological impact studies (e.g., Defries, Bounoua, & Collatz, 2002; Feddema et al., 2005; Maynard & Royer, 2004). Even though progress has been made during the last decade by systematically improving the resolution of the scenarios (e.g., Zhang, Justice, Jiang, Brunner, & Wilkie, 2006), spatially explicit deforestation scenarios are still mostly binary (i.e., indicating grid cells which are converted from forest to non-forest). The scenarios are suitable to be implemented *as such* in the older-generation simple climatological and environmental models (Figure 1(a)).

With the possibility of including a more complex land surface in recent state-of-the-art models (e.g., Community Land Model; Oleson et al., 2010), there is a growing need for more detailed deforestation scenarios: a reference land grid cell is no longer an homogeneous unit and can contain, not just one, but several land cover types ("Plant Functional Types" or "PFT's"): this is the so-called *tile approach.* Its difference with the simple models is depicted in Figure 1 (compare left panels in 1(a) and (b)). The advantage of this approach is that, even with a large horizontal land grid cell resolution of around 50 km, the impact of a certain areal proportion of different land-cover types (e.g., on the regional climate) can be simulated. Hence, when implementing a deforestation scenario in complex tile-using models (Figure 1(b)), it is no longer sufficient to know how much and where deforestation takes place (as usually provided by the scenario), but ideally also where successional vegetation types occur in place and in which relative proportions (i.e., *multiple-class forest conversion*, cf. arrow (2) in Figure 1(b)). If this information is lacking, the implementation of the scenario should be undertaken using a *single-class forest conversion* by assuming one successional land-cover type for the entire deforested area, for which soil or cropland is usually chosen (cf. arrow (1) in Figure 1(b)).

Studies have been performed on tropical fallow succession after rainforest clearing, including a detailed description of fallow stages, duration, and temporal evolution (Bazzaz & Pickett, 1980; Styger, Rakotondramasy, Pfeffer, Fernandes, & Bates, 2007) and more specifically for the Congo Basin (Lebamba et al., 2009; Makana & Thomas, 2006). Styger et al. (2007) demonstrated the importance of cultivation history and time since deforestation for the characterization of fallow vegetation. However, none of these studies quantify the relative areal proportions of different succession stages: how much cleared land is typically occupied by crop fields, young fallow, or new forest? The only source of information, especially for the Congo Basin rainforest, is the geographical information system (GIS) literature, such as remote sensing studies, discussing image classification with single-moment (or "snapshot") distributions of land-cover classes (Mayaux, De Grandi, & Malingreau, 2000; Vancutsem, Pekel, Evrard, Malaisse, & Defourny, 2009). However, in contrast to the above-mentioned studies on fallow succession, GIS studies are limited in describing the land-cover classes and often group successional vegetation together in a single class (e.g., rural complex, agricultural matrix).

The main aim of this study is to address these issues by identifying the present-day successional land-cover types and quantifying their areal proportions. Using GIS, this is

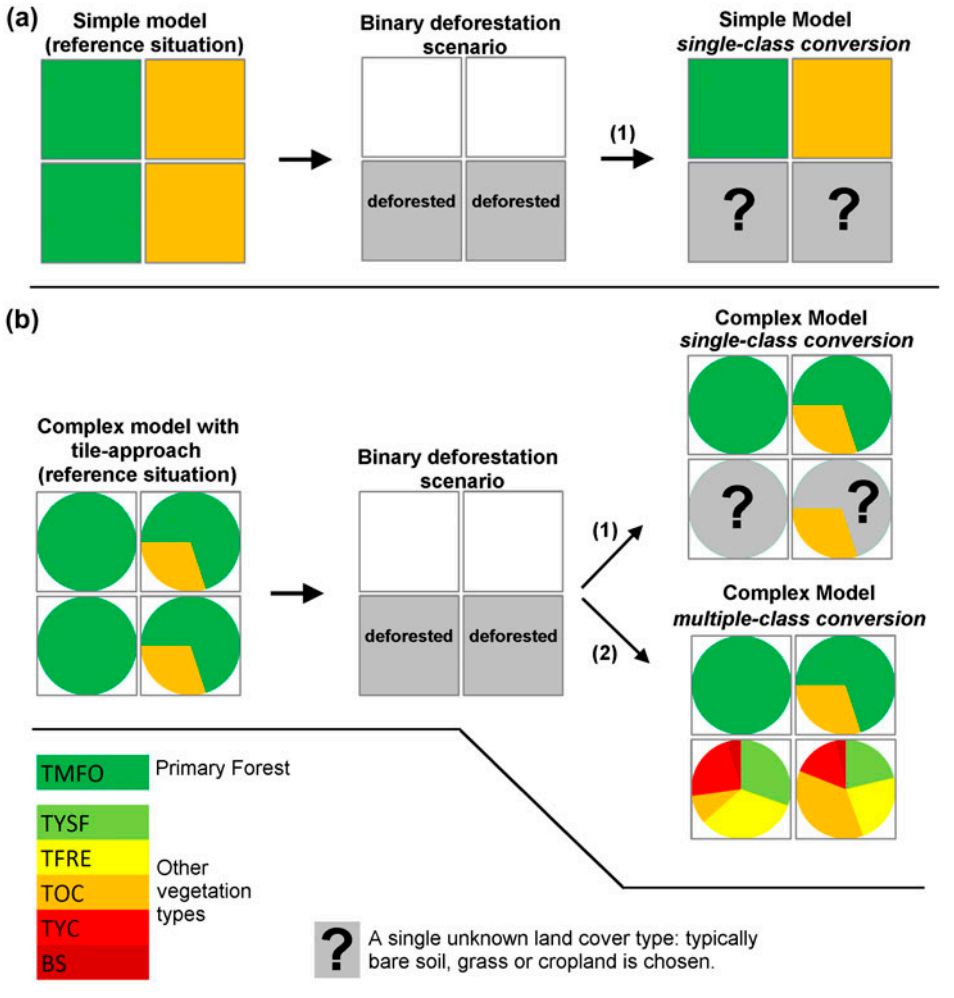

Figure 1. Implementation of a binary deforestation scenario in four grid cells of a (a) simple model and (b) complex or tile-approach model. In the reference situation of the complex model (left panel), the two grid cells on the left have initially a 100% forest cover and the two grid cells to the right have only 70%. The implementation of the scenario (right panels) can be done by (1) converting forest to a single non-forest land-cover type (question marks), assigned to, for example, BS or cropland (single-class conversion), or (2) by replacing the forest by a mosaic of successional land-cover types with areal proportions as e.g., derived from this study (multiple-class conversion). TMFO = Tropical Mature Forest. Other acronyms are successional vegetation stages.

achieved by combining a detection of historically deforested areas with a present-day classified land-cover map (including explicit representation of the successional fallow cycle). Secondly, an additional objective of this study is to calculate these proportions for areas with different deforestation age, since the characterization of successional vegetation types is related to time since deforestation (Styger et al., 2007). This relation is investigated by categorizing the deforested region in three areas according to time since deforestation, in near-decadal deforestation periods. Ideally, denser time series,

and hence more deforestation periods, are used for this purpose; however, this was not possible due to the excessive cloudiness in equatorial rainforest regions, resulting in a limited availability of Landsat scenes free of clouds and artifacts.

Existing binary deforestation scenarios can then be complemented with these successional land-cover types and their areal proportions through *multiple-class forest conversion* (arrow (2) in Figure 1(b)). Through this approach, the discrepancy between the supply side (binary deforestation scenarios on a coarse resolution) and demand side (more complex models requiring detailed scenarios) is bridged. Recent climatological studies, in particular, are trying to quantify the impact of deforestation such that it is "as realistic as possible" (e.g., Maynard & Royer, 2004); this objective is, however, limited by the binary nature of the available scenarios (i.e., forest to non-forest) only allowing *single-class forest conversion* (arrow (1) in Figure 1(b)). Knowledge about the typical successional vegetation types and their relative areal proportions is therefore necessary and could, if available, improve the degree of realism in such climatological studies.

Complementing deforestation scenarios with *multiple-class forest conversion* is especially important when considering a diverse patchwork of successional land-cover types. Since this is the case for shifting cultivation systems, as typically observed in Central Africa (Russell, Mbile, & Tchamou, 2011), the frontier zone of the Congo Basin rainforest is a suitable study area. Furthermore, the Congo Basin rainforest is the second largest dense tropical forest in the world, and despite the projections of high population growth and potential deforestation pressure (Zhang et al., 2006), only a few modeling studies have investigated the climatological impact of deforestation in this region (Maynard & Royer, 2004), compared to the other major rainforest regions.

In this paper, Section 2 documents the study area and the data sources used. Section 3 covers the most important methodological steps in the analyzes, including the definition of vegetation classes used in the supervised classification. Section 4 provides a chronological sequence of auxiliary and main results: first, a deforestation age assessment was conducted, in which historical deforestation was detected and mapped (Section 4.1). Subsequently, the present-day land cover was classified in a number of detailed land-cover classes and then validated (Section 4.2). The main objective, however, was the identification of present-day successional land-cover types and the quantification of their areal proportions, presented in Section 4.3. The present-day land cover is related to the areas of historical deforestation, and, from that, a relative distribution of present-day land-cover classes was derived. The second objective was to investigate the dependency on time since deforestation, which is also shown in this section. Finally, Section 4.4 illustrates and quantifies the use of the previously obtained main results by projecting gridded fields of two ecological parameters (LAI and canopy height (CH)) to the year 2050 according to an existing deforestation scenario: first with a *single-class conversion* (forest-to-crops) and second with a *multiple-class conversion* by assessing the area of forest removal to a mosaic of successional land-cover classes with relative areal proportions derived from this study.

2. Materials

2.1. Study area

Kisangani (0°31′0″N 25°12′0″E) is the third largest city of the D.R. Congo and the largest urbanized center in the midst of the vast Congo Basin rainforest (Figure 2). Outside the urban center, the rural population has, since colonial times, concentrated

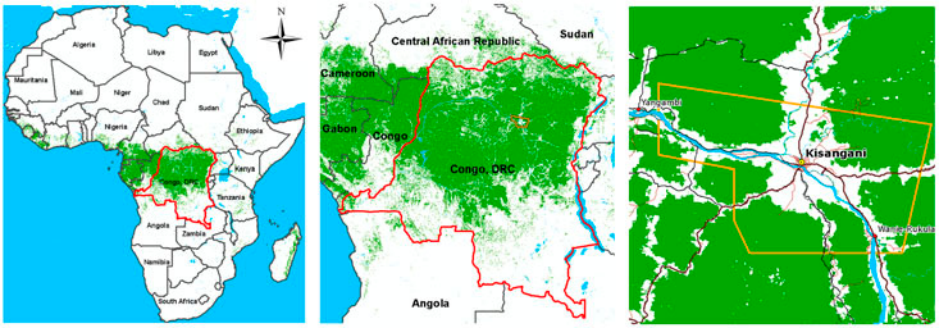

Figure 2. Location of study area. Red: D.R. Congo; Orange: Cutout of Landsat image 170/060 for analysis. Green: Dense humid forest of Central Africa (FACET, 2010).

along the major transport axes (roads and navigable rivers) in typical, linearly constructed villages. The livelihood of the people is derived from a diverse array of activities of which slash-and-burn agriculture is practiced by the majority of households (also referred to as *swidden agriculture* or *shifting cultivation*) (Russell et al., 2011). The agricultural system results in a shifting patchwork of cultivated fields, fallows, secondary forests, and remnants of primary forests. Agriculture is primarily practiced for subsistence (typical crops are cassava and plantain) but, with the main cash crop being rice, market-oriented production is also important in the study area, as Kisangani is relatively nearby. Forest clearing for agriculture is intensifying, due to population growth in Kisangani and villages, and forms the principal driver of deforestation in the Congo Basin rainforest (Norris et al., 2010). This scale is in contrast to that of many other tropical forests (e.g., the Amazon), where industrial-scale clearing is more important and is focused on large-scale agriculture and cattle ranching (Butler & Laurance, 2008). Artisanal charcoal production is an additional but minor contributor to wood logging activities that result in forest degradation.

2.2. Data

2.2.1. Remote sensing imagery

This study is based on a selection of one Landsat Multispectral Scanning System (MSS; 1975), two Thematic Mapper (TM; 1990, 2001), and one Enhanced TM (ETM+; 2012) image(s) from scene 176/060 located in the D.R. Congo and containing the city of Kisangani with its surrounding rainforest (Figure 2). The image of 1975 (MSS) has a native grid-cell resolution of 60 m; the other three images (TM/ETM+) are more detailed, with a resolution of 30 m. Acquisition dates providing cloud-free imagery were mainly during the driest month (January, 53 mm/month), although the 2001 image was acquired in March. As the dry period is short, with less than 60 mm precipitation, the region is classified as a tropical monsoon climate, despite its proximity to the Equator and an average annual precipitation of 1620 mm and relative humidity of 86%.

Prior to any analysis, we converted all four images (1975, 1990, 2001, and 2012) from raw digital numbers to top-of-atmosphere (TOA) reflectance values (%) by applying a radiometric correction, which makes use of acquisition date and sun elevation to calculate image-specific conversion parameters (offset and gain). This procedure

largely removes differences due to solar zenith angle, earth-sun distance, and sensor differences between multi-temporal image series (Bruce & Hilbert, 2006). Correction of TOA reflectance to surface reflectance is not necessary when considering image classification and post-classification change detection (Song, Woodcock, Seto, Lenney, & Macomber, 2001). This is the case in our analysis, hence we omitted such correction in the data pre-processing.

2.2.2. *Collected and post-processed data from field campaign*

An observational field campaign was conducted between 13 May 2012 and 4 June 2012 throughout recently (0–35 year) deforested areas up to the forest frontier. On a regular basis, we recorded ground-truth points describing the dominant land cover and noted their geographical position within the forest frontier zone, spatially spread as much as possible across the study area (Figure 3), with a total sample size of 1785 data points. We used the data obtained to validate the supervised image classification, which focused on different successional classes.

Furthermore, we observed tree height and leaf area index (LAI). We used these data to validate an existing gridded data-set of CH and LAI for primary forest (Section 2.2.3) and to derive these parameters for young secondary forest (TYSF), which is not represented in the data-set. The gridded data are used in the illustrative application of the results (Section 4.4). Observations were only undertaken for vegetation types containing closed-canopy trees, which ranged from TYSF to mature forest.

CH was measured directly using a hand-held laser altimeter, with sample sizes n = 136 and 58 for TYSF and mature forest, respectively. Simultaneously, we

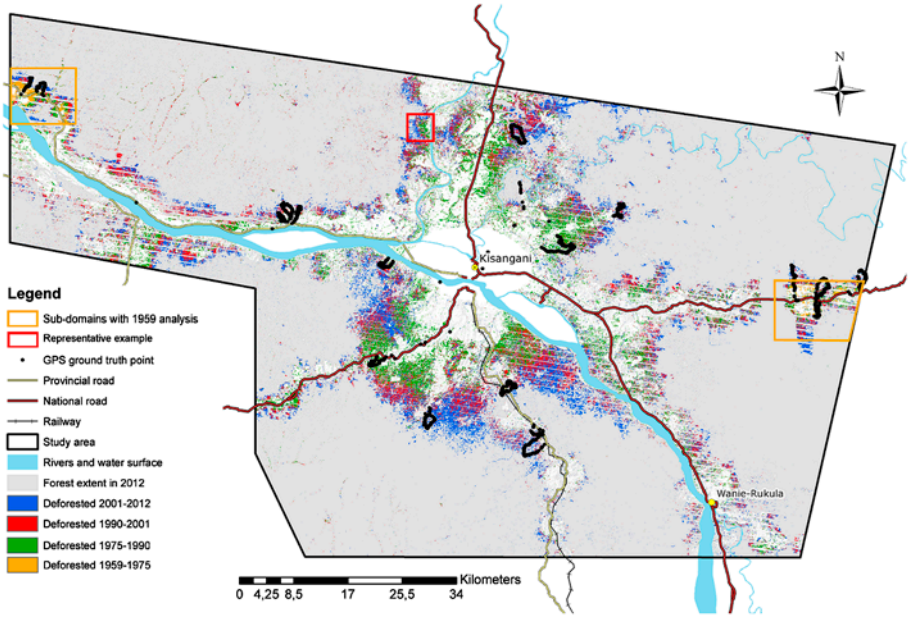

Figure 3. Overview map. The red square indicates a representative example, shown in detail in Figure 7, and orange squares indicate two sub-regions in which the analyzes are also done for the period 1959–1975. Black dots are ground truth points describing the dominant land cover.

observed canopy light transmittance indirectly by taking the proportion of below-canopy to above-canopy light (Q_i/Q_0), measured using a hand-held photometer. The relation between light transmittance and LAI is described by the Beer–Lambert law (Equation (1)):

$$\mathrm{LAI} = -\mathrm{In}\left(\frac{Q_i}{Q_0}\right) \cdot k^{-1} \quad (1)$$

Only the extinction coefficient (k) has to be known. The dimensionless coefficient characterizes the interception and distribution of light by the canopy and its vertical attenuation through the vegetation crown. The extinction coefficient depends on vegetation type. For mature forest, we used the mean value as found by Wirth, Weber, and Ryel (2001), which is 0.78. Although early species in tropical vegetation succession are characterized by a lower LAI, they tend to have higher extinction coefficients (Kitajima, Mulkey, & Wright, 2005). Hence, for TYSF, we took the highest value of k found in the literature for tropical vegetation, being 0.88 (Cournac, Dubois, Chave, & Riéra, 2002; Emmons et al., 2006).

2.2.3. *Gridded data-sets of LAI and CH*

LAI and CH are provided in a spatially explicit gridded data-set of Lawrence and Chase (2007) for 17 PFT's using a *tile approach*. The data are derived from MODIS imagery with a horizontal resolution of 5×5 km. Common tropical PFT's in the data-set are BS, crops, grass, and broad-leaved tropical evergreen forest (Figure 4(a)). Each grid cell can contain multiple PFT's with a certain areal proportion, defining the grid-cell-averaged ecological parameters (e.g., CH in a given grid cell is calculated as areally weighted average of PFT-specific values for CH in the cell). Typically, a densely forested grid cell is composed of about 70–80% primary forest complemented by a remainder of grass and/or small trees, on average resulting in a grid-cell-averaged CH of 25.5 m and LAI of 4.3 m²/m². Maps with the present-day reference situation of gridded CH (CH_{2000}), and (LAI_{2000}) are shown in Figure 4(c) and (d).

3. Methodology

The main objective of this study was to calculate relative areal proportions of present-day successional land-cover classes, which can be used subsequently to complement future binary deforestation scenarios with a *multiple-class conversion* of forest, instead of the less accurate *single-class conversion* of forest to a single successional land cover. The methods used to achieve this objective are shown in a conceptual flowchart (Figure 5), which also shows the corresponding auxiliary and main results.

3.1. *Deforestation age assessment*

Primary forest in each image (1975, 1990, 2001, and 2012) is discriminated from a remainder class using the unsupervised ISODATA technique (Ball & Hall, 1965). The term "deforestation" is used in this study to indicate the anthropogenic transition from primary forest to any other non-primary forest land-cover type. We then created three deforestation maps by subtracting each consecutive pair of forest maps from each other, resulting in maps of deforested area from 1975–1990, 1990–2001, and 2001–2012 ("deforestation age assessment"; arrow (3.1) in Figure 5). From these maps, we

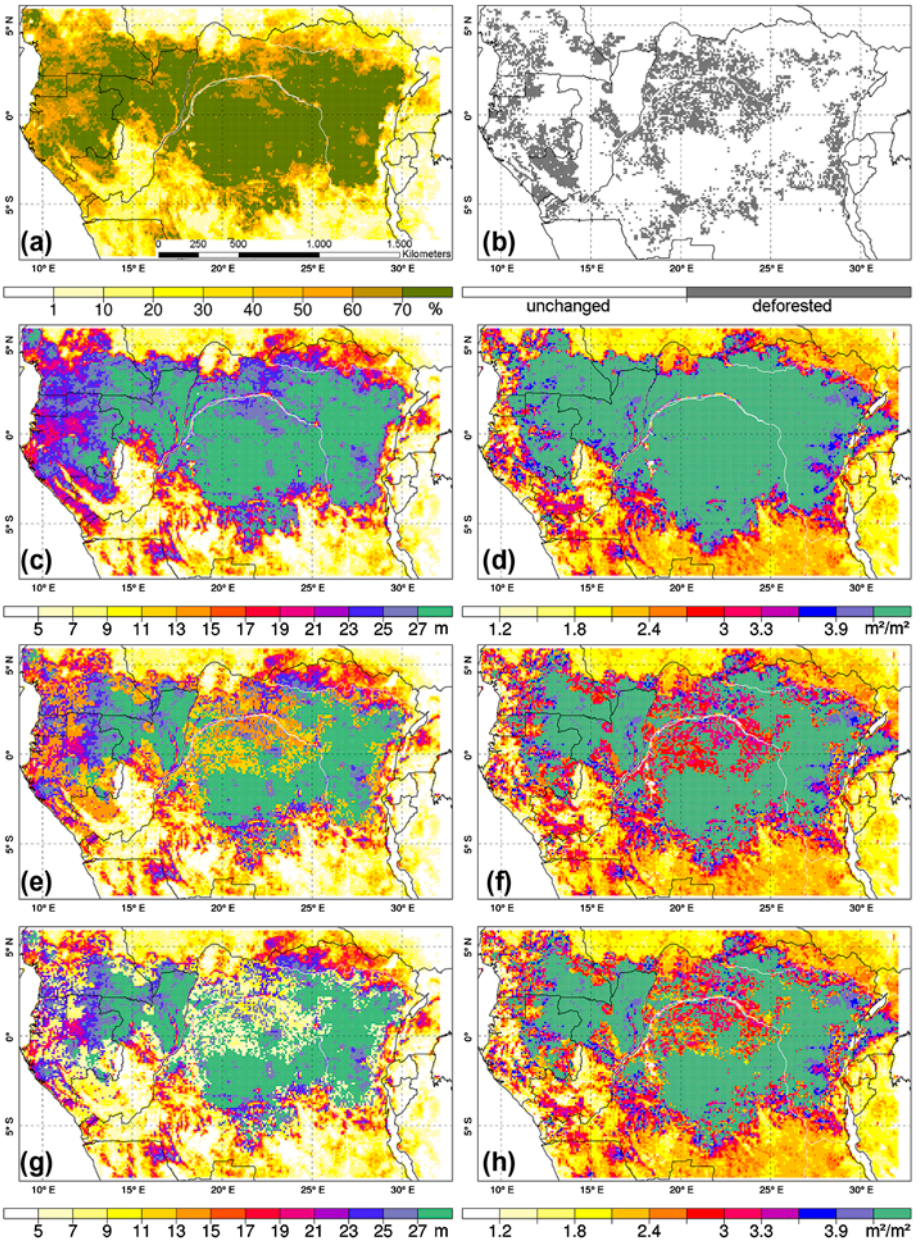

Figure 4. (a) Initial areal percentage of the PFT "Broadleaf Evergreen Tropical Forest" in each grid cell; (b) binary future deforestation scenario for 2050 of Zhang et al. (2006); (c–d) reference situation: gridcell-averaged CH (c) and LAI (d) (CH_{2000} from Lawrence & Chase, 2007); (e–f) future projection of CH (e) and LAI (f) (CH_{2050} and LAI_{2050}) using the scenario of Zhang et al. (2006), replacing the portion primary forest in every grid cell by a mix of successional vegetation types (*multiple-class conversion*); and (g–h) A12050 calculated by converting the portion primary forest in every grid cell to cropland (*single-class conversion*).

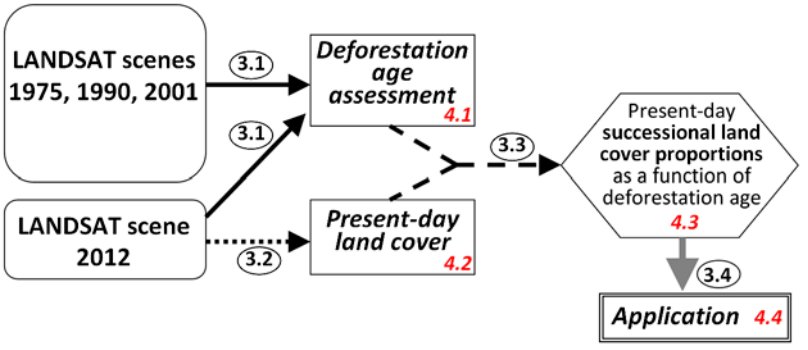

Figure 5. Methodological flowchart. Black solid arrows indicate the unsupervised ISODATA identification of primary forest, resulting in near-decadal deforestation maps allowing the assessment of deforestation age and the calculation of their respective deforested areas. The dotted arrow indicates the supervised classification, which resulted in a present-day land cover map; the broken arrow indicates the extraction of present-day land-cover proportions for each deforestation period; the thick gray arrow indicates the implementation of the main results in an illustrative application. Numbers in circles represent the methodological sections covering the different processes and red numbers in italics represent the sections discussing the respective results.

calculated the absolute deforested area (km²), as well as deforestation rate per period (km²/year). The rates are temporal averages (time-normalized), which makes deforestation in the different periods comparable. To make sure that no false deforestation is taken into account, only grid cells with a single and permanent shift from primary forest to any other land-cover class (either during 1975–1990, 1990–2001, or 2001–2012) are considered "deforested." The image of 2012 has artifacts in the form of stripes: due to the above-mentioned restriction, these artifacts propagate to the maps of all three deforestation periods; however, they do not influence the results quantitatively since they are evenly distributed over the image and are not taken into account for any of the analyzes (the grid cells affected by stripes were marked "invalid" and not included in the subsequent calculations and algorithms).

Aerial photographs from 1959 were used to complement the Landsat analyzes in two small sub-domains, allowing extension of the analysis back in time. We stitched together and georeferenced the photographs and digitized polygons containing primary forest. We then rasterized the vector maps to Landsat-sized pixels in order to compare them quantitatively with the other maps.

3.2. *Supervised classification of present-day land cover*

3.2.1. *Defining vegetation classes*

Different vegetation classes were defined *a priori*. Where possible, we did this using existing studies on successional fallow stages observed in tropical Africa: Styger et al. (2007) analyzed tropical vegetation succession after rainforest clearing in Madagascar and discriminated different fallow stages with their own specific characteristics, and Lebamba et al. (2009) derived forest succession stages from pollen data in Central Africa, partly resulting in the same fallow stages as found by Styger et al. (2007).

Classes used in this study were BS, tropical young cultivated (TYC), tropical old cultivated (TOC), tropical forest regrowth (TFRE), tropical TYSF, and tropical mature or primary forest (TMFO) (Figure 6). An overview of class descriptions from Styger

et al. (2007) and Lebamba et al. (2009) is complemented with additional information and provided in Table 1.

All the classes are successional fallow stages (Figure 6(c)) and are part of a continuous cycle of subsequent land-cover changes caused by the shifting cultivation system after initial removal of primary forest (when TMFO is converted to BS): each plot of land within the shifting-cultivation patchwork (located in between the village and the rainforest) can at any time be situated in one of these stages. A cycle starts directly after initial deforestation and, often with declining intensity, persists until the present day (Van Vliet et al., 2012). Transitions from BS to TYSF are constructive (i.e., caused by growing and changing vegetation type), while the transition from TYSF to BS is destructive since it represents the anthropogenic removal (slashing and burning) of tree fallows to initiate a new cultivated field.

The old secondary forest stage (TOSF) is not included in this study. Although this land-cover type is occasionally present in the study area, it is mostly concentrated in forest reserves and protected areas; it is not found along the major recent (0–35 year) deforestation axes, and the observation frequency during the field campaign was of marginal significance. This state can be explained by the high deforestation pressure that currently exists in the region and the time needed to reach the TOSF stage (around 30–40 year): before a swidden plot gets the chance to develop to this stage, it is already incorporated in a new fallow cycle (Figure 6(c)).

3.2.2. *Classification procedure*

The Landsat image of 2012 was used to create a present-day land-cover map (arrow (3.2) in Figure 5) by using the maximum likelihood technique (Richards, 1999) and delineating training areas for the discretized fallow vegetation stages (Section 3.2.1), roads, and water surfaces. We undertook this with the aid of high-resolution imagery (through Google Earth and WorldView images), visual interpretation, and expert knowledge from the field campaign. The high-resolution images were first compared with the ground-truth points to verify that the correct vegetation could be recognized from these images and then used to select large areas of homogeneous land cover to delineate corresponding polygons on the Landsat images. This procedure needed careful interpretation since acquisition dates of high-resolution imagery were mainly from April 2011. Hence, only older vegetation stages, which most likely did not develop into a next fallow stage during the one year, could be identified using this method. For recent forest clearings (between 2011 and 2012) and younger and more dynamic vegetation stages, only a direct comparison of *in situ* data and Landsat imagery was possible.

3.2.3. *Classification validation*

After establishing the vegetation classes and classification of the present-day image, validation of the classified image was undertaken using standard confusion matrices.

A time lag of 3.5–4.5 months existed between the Landsat image acquisition (29 January 2012) and registration of the ground-truth points. Since vegetation grows much faster than in temperate environments, it is difficult to use ground-truth points for dynamic (younger) stages, which probably changed drastically during the time lag, with transition times of months. For instance, BS is very quickly covered with pioneer herbs, crop fields have a rapid development from almost BS to completely covered soil, and young fallow can develop quickly into medium fallow. For these classes, validation

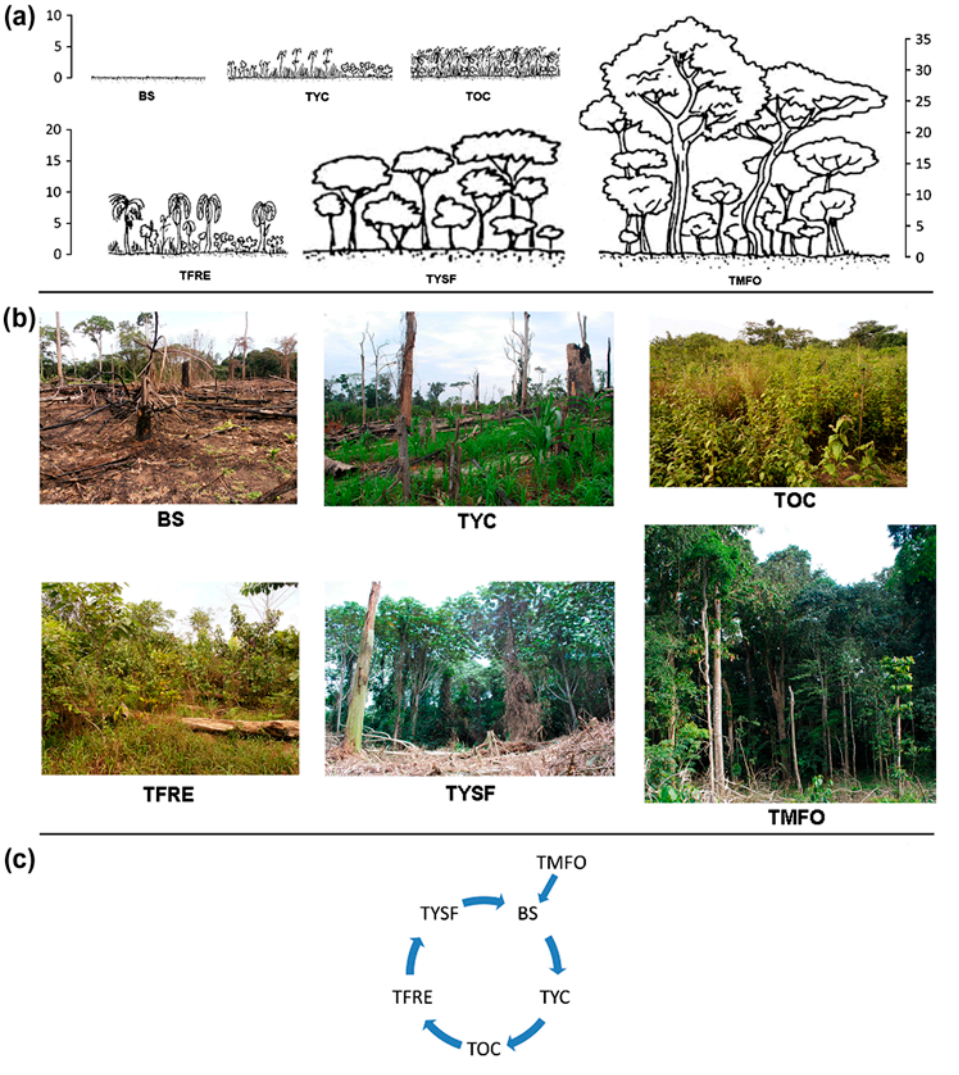

Figure 6. (a) Vegetation classes used in this study, scaled by height. Adapted from Dobois (1996). BS: Bare Soil; TYC: Tropical Young Cultivated; TOC: Tropical Old Cultivated; TFRE: Tropical Forest Regrowth; TYSF: Tropical Young Secondary Forest; and TMFO: Tropical Mature Forest. (b) Vegetation classes used in this study, photographed during field campaign. (c) Successional fallow cycle.

was performed using independent and randomly chosen test polygons from the same Landsat image.

We validated classification of land-cover types that are more stable and less likely to have changed during the lag time (TFRE, TYSF, and TMFO), with transition times of years, with observed ground-truth points.

3.3. *Relating present-day land-cover proportions to deforestation age*

The evaluated classified image was then ready and approved to extract areal proportions of present-day successional vegetation classes for each deforestation period

Table 1. Overview of land cover classes mentioned in this study, Styger et al. (2007) and Lebamba et al. (2009).

Class	Name	Styger et al. (2007)	Lebamba et al. (2009)	Additional information
BS	Bare soil	/	/	Bare soil, possibly including dead vegetation (cut and/or burned canopies)
TYC	Tropical Young Cultivated		/	Young crop fields with the soil still partly exposed. Also, this category belong pioneer herbs and degraded Savannah-like grasslands: they are spectrally similar since their canopy structure does not cover the soil completely
TOC	Tropical Old Cultivated	Immature Shrub Fallow or *Ramarasana/ Dedeka* stage	Grass herbaceous to semi-woody stage	Older and taller than TYC, often corresponds with abandoned crop fields, interwoven with and overgrown by herbaceous weeds and semi-woody plants. The underlying soil is not visible
TFRE*	Tropical Forest Regrowth	Mature Shrub Fallow or *Savoka* stage	Corresponding to the forest woody regrowth stage. In this stage, the dominant shrubs and small trees, mainly heliophilous, such as *Albizia, Anthocleista, Harungana, Tetrorchidium, Trema,* and *Vernonia conferta* are mixed with many coarse herbs (e.g., *Zingiberaceae*), soft woody shrubs, and small climbers (e.g., *Dioscorea*)	Open canopy crown, tree height 7–11 m**. Age between 2 and 5 years
TYSF*	Tropical Young Secondary Forest	Tree Fallow or *Savoka Mody's* stage	Characteristically this young secondary stage is dominated by the fast growing *heliophilous Musanga cecropioides* which is the most abundant and characteristic secondary forest tree in tropical Africa, associated with *Myrianthus, Macaranga,* or *Albizia* for the most abundant trees. The herbaceous and shrubby layer are dense and lianas are abundant (e.g., *Apocynaceae*)	Closed canopy crown, tree height 12–25 m**. Age between 5 and 20 years
TOSF*	Tropical Old Secondary Forest	*Ala Ordinaire* stage	This old secondary stage is dominated by semiheliophilous species of moderately rapid growth. Characteristic species occurring in the canopy are: *Alstonia boonei, Canarium, Ceiba pentandra, Zanthoxylum macrophylllum, Pycnanthus angolensis, Terminalia superba, and Triplochiton scleroxylon*	Age between 30 and 40 years*Not used in this study*

(*Continued*)

Table 1. (*Continued*).

Class	Name	Styger et al. (2007)	Lebamba et al. (2009)	Additional information
TMFO*	Tropical Mature Forest	*Aty Ala* stage	This is the ultimate stage, or climactic mature stage, of forest regeneration. The floristic composition of this forest stage, the presence of shrub and herbaceous strata depends on the status of the forest: semi-deciduous or mixed semi-evergreen	Age >50 years, tree height >27 m

*Acronym of land cover class is literally taken from Lebamba et al. (2009).
**Taken from measurements in the field campaign.

(arrow (3.3) in Figure 5). In the Amazon and Indonesian rainforest, swidden plots are mostly converted to a permanent land cover, such as pasture grassland, annual crops, managed stands, and fruit plantations (Van Vliet et al., 2012). In the Congo Basin rainforest, however, almost all areas that were deforested for slash-and-burn practices also remained in the shifting cultivation cycle until total degradation (Van Vliet et al., 2012). Given the fast growth rates in an equatorial climate and relatively short fallow duration, comparing two satellite images of the region with a relatively small time lag (a few months) will yield a highly variable spatial distribution of land-cover types (i.e., stages of fallow succession). Therefore, it is more important to quantify the relative areal contribution of each succession stage to the total deforested area, rather than the exact spatial pattern. This is in accordance with our main objective to capture the long-term relative proportions of fallow stages (existing within the deforested area) instead of the short-term dynamics (such as annual reclearance and regeneration).

3.4. *Illustrative application of the main results*

The main objective of this study was to quantify relative areal proportions of successional vegetation types. A useful application of these results is *multiple-class* conversion of forest in binary deforestation scenarios, of which the difference with single-class conversion is shown in Figure 1(b). The following section aims to illustrate the advantage of implementing an existing deforestation scenario using *multiple-class* conversion (forest to a range of successional vegetation PFT's) compared to *single-class* conversion (forest-to-crops only). Therefore, we projected gridded reference data-sets of CH and LAI (Section 2.2.3) to the future using a binary deforestation scenario. Although being of less topical interest than above-ground biomass or carbon stocks, LAI and CH are widely used within the environmental modeling community; these basic parameters are better supported by observations and have a large indirect influence through many other dependent parameters (e.g., roughness length, rainfall interception, canopy transmittance) on the output results of models. Zhang et al. (2006) provided a simple binary deforestation projection of 2050 (Figure 4(b)), which we refined, using the results obtained in our study, through *multiple-class* conversion. As a result, more realistic post-deforestation grid-cell-averages are expected.

First, we used observations to validate the information about primary forest in the reference data-set and to construct information for the vegetation type TYSF, which is not available in the reference data-set. Then, implementation of the deforestation scenario was initiated by removing the portion of existing primary forest (Figure 4(a)) within grid cells corresponding to the deforested cells in Zhang et al. (2006; Figure 4(b)). In the first case, it was replaced by a single land-cover type – crops (*single-class* forest conversion) – as undertaken in many deforestation studies. In the second case, it was replaced by a combination of successional fallow vegetation classes (*multiple-class* conversion), of which the average internal areal proportions will be provided by this study (e.g., *x*% BS, *y*% cropland, *z*% TYSF). In both cases, all existing forest within deforested grid cells is removed and replaced.

Post-deforestation grid-cell-averaged CH and LAI were composed as explained in Section 2.2.3, but included two new vegetation types, TYSF and TFRE, which were not in the reference data-set of Lawrence and Chase (2007). We based LAI_{TYSF} on measurements from the field campaign. As a spatially varying gridded field is preferred over a single constant, we used the average proportion of LAI_{TYSF}/LAI_{TMFO} (51%) to calculate LAI_{TYSF} from the spatially varying field LAI_{TMFO}. Since LAI_{TYSF} is never

lower than the LAI of crops or grass, an additional constraint was added by taking the maximum of all:

$$\mathrm{LAI_{TYSF}} = \max(\mathrm{LAI_{TYC}}, \mathrm{LAI_{TOC}}, 0.51 \cdot \mathrm{LAI_{TMFO}}) \quad (2)$$

TFRE, the stage between low vegetation and TYSF did not correspond as well to an existing PFT in the reference data-set. Therefore, $\mathrm{LAI_{TFRE}}$ was based on the fact that the land-cover class is a transitional mix between TOC and TYSF:

$$\mathrm{LAI_{TFRE}} = \mathrm{mean}(\mathrm{LAI_{TOC}}, \mathrm{LAI_{TYSF}}) \quad (3)$$

The same method was used to calculate the PFT-specific gridded fields $\mathrm{CH_{TYSF}}$ and $\mathrm{CH_{TFRE}}$.

4. Results

Auxiliary results (Sections 4.1 and 4.2) and main results (Section 4.3) discussed, hereafter, are represented in the same flow chart as used in the methodology section (Figure 5). An additional section illustrates the use of our results in an application (Section 4.4).

4.1. *Deforestation age assessment*

The recently deforested areas are mostly situated near the frontier of the primary forest, while the older deforested areas are located closer to the city or transport axes (rivers and roads) as shown in Figure 3. A representative example is the Lindi River to the north of Kisangani (Figure 7). This transport axis increases accessibility and the population density is correspondingly high. The increased local need for agricultural land explains the presence of a "deforestation front" advancing from the river towards the rainforest. In this specific case, the local deforested area and rate were higher during the periods 1975–1990 and 2001–2012, and lower between 1990 and 2001.

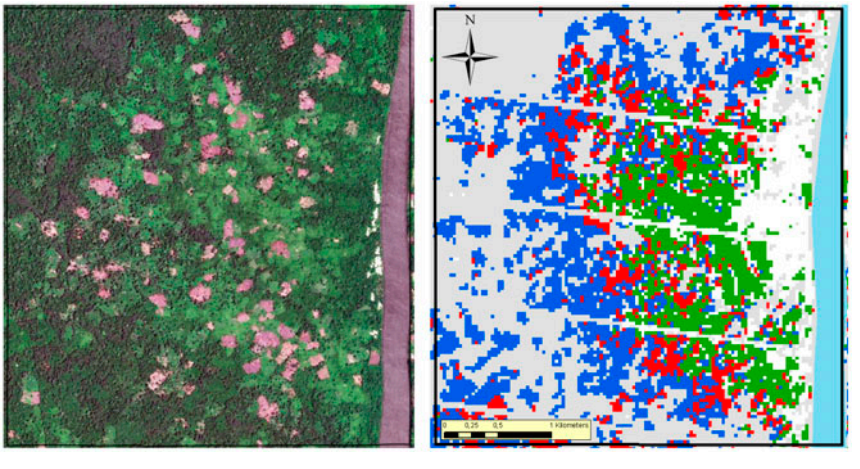

Figure 7. Representative example: high-resolution image (left), deforestation areas as indicated in Figure 3 (right) with deforestation during 1975–1990 (green), 1990s–2001 (red), and 2001–2012 (blue). Note the subtle differences between black green primary forest and dark green TYSF in the high-resolution image.

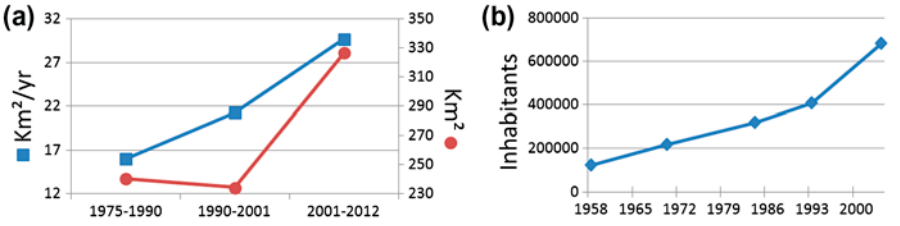

Figure 8. (a) Average deforestation rate (km²/year) and absolute deforested area (km²) in the study area during each deforestation period. (b) Evolution of the population in Kisangani.

Average deforestation rate shows an almost linear increase (Figure 8(a)), which is related to the population growth in Kisangani (Figure 8(b)) as shown by Bamba, Barima, and Bogaert (2010). We note that these rates are temporally averaged over each of the three periods and hence subject to uncertainty due to internal temporal variability (most deforestation randomly happened within such a period without taking the complete time of that period). Most importantly, however, averaging makes the deforestation during the three subsequent periods comparable.

4.2. *Classification of present-day land cover*

4.2.1. *The present-day land-cover map*

A representative example of the entire present-day land-cover map illustrates the heavily scattered land-cover pattern (Figure 9). The classified map shows the obvious relation between small streams and the presence of untouched forest. However, obstacles such as these streams (and also steep slopes) can only canalize the deforestation patterns temporarily: when the pressure of finding new agricultural land is too high, the obstacles are crossed or bypassed, and the deforestation front advances further forest-inwards.

The study area has 70% of its dry surface covered with primary forest. Almost equally important are TYSF (9%) and TFRE or medium fallow (10%). Agricultural land and degraded savanna-like grasslands occupy approximately 6% of the land surface, and the smallest area is covered by abandoned cropfields (or young fallow) and BS with, respectively, 3 and 2%.

4.2.2. *Validation of present-day image classification*

Best classification performance was found for water surfaces, followed by old cultivations, BS and roads, and young cultivated fields, then, in decreasing order of accuracy, by primary forest, TYSF, and TFRE (Table 2). Classes validated with test-polygons (BS, TYC, and TOC) show good performance, with producers' and users' accuracy of 85% and higher. Classes validated with ground-truth points (TFRE, TYSF, and TMFO) have lower accuracy (60–85%), for two reasons. First, these classes are more difficult to classify because their spectral intra-class variance and inter-class overlap are higher compared to classes, such as roads and water surfaces. Second, the ground-truth points themselves are a source of uncertainty: during the time lag between image acquisition and terrain observation (3.5–4.5 months), some of the observed plots could have shifted to a next successional stage, even when only considering the

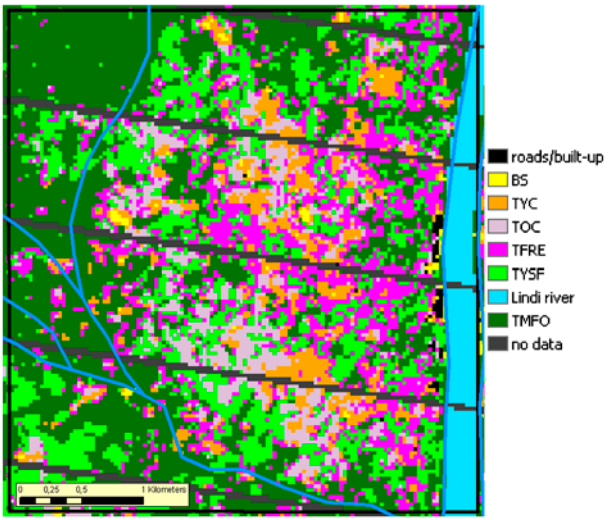

Figure 9. Representative example with land-cover classification of the present-day Landsat image (2012). Small-scale hydrography is shown with blue lines.

Table 2. Performance statistics from classification of 2012 image. PA = Producers' Accuracy, UA = Users' Accuracy. Red/bold numbers are the result of ground-truth-point validation, the rest of the classes are validated using separate calibration and validation areas.

	PA (%)	UA (%)
Water	99.19	100.00
Roads	100.00	94.20
TFRE	63.39	62.83
TYSF	71.01	76.43
TMFO	85.09	82.20
TOC	96.43	99.12
TYC	93.62	87.74
BS	98.45	89.44

"stable" land-cover types, which could partly explain the gradual increase of accuracy with stage (TFRE < TYSF < TMFO).

We additionally validated TMFO by calculating the percentage of spatial overlap between supervised-classified TMFO (Section 4.2.1) and unsupervised, classified TMFO (Section 4.1). The 97% correspondence justifies the unsupervised classification ISODATA technique discussed in earlier sections. The overall accuracy (94.4312%) and Kappa coefficient (0.9221) indicate an excellent overall agreement (Ortiz, Formaggio, & Epiphanio, 1997).

4.3. Relating present-day successional land-cover proportions to deforestation age

For the main objective of this study – assessment of the amount of each post-clearing successional land-cover type relative to the total deforested area ("areal land-cover proportion") – the classes "BS" (recently cleared plots) and "roads" were merged in

"BS" since their individual share was very small and, in reality, the (mostly sandy) roads indeed consist of unvegetated soil.

First, the results are generalized by ignoring the dependency on time since deforestation and by calculating the average present-day areal share of each land-cover type to the total area deforested between 1975 and 2012. We then obtained 4.9% BS, 22.3% TYC, 9.4% TOC, 33.1% TFRE, and 30.4% TYSF. These numbers can be used to express the proportions of successional vegetation types in any tile-approach grid cell from environmental and climatological models, as illustrated in Figure 1(b).

The areal proportion of each land-cover class depends on the transition rates within the successional fallow cycle (Figure 6(c)), and hence evolves over time. A higher present-day areal share of degraded grassland and TYC, and of abandoned TOC, is found in areas deforested a longer time ago (Figure 10): together, their combined areal proportion of total deforested area increases from around 25 (in areas deforested during 2001–2012) to 38% (in areas deforested during 1975–1990). The TFRE does not show a clear trend or correlation with time since deforestation. A marked lower present-day areal share of TYSF exists in areas that were deforested a longer time ago: TYSF amounts for 36% of the area deforested during 2001–2012 and only 20% of the area

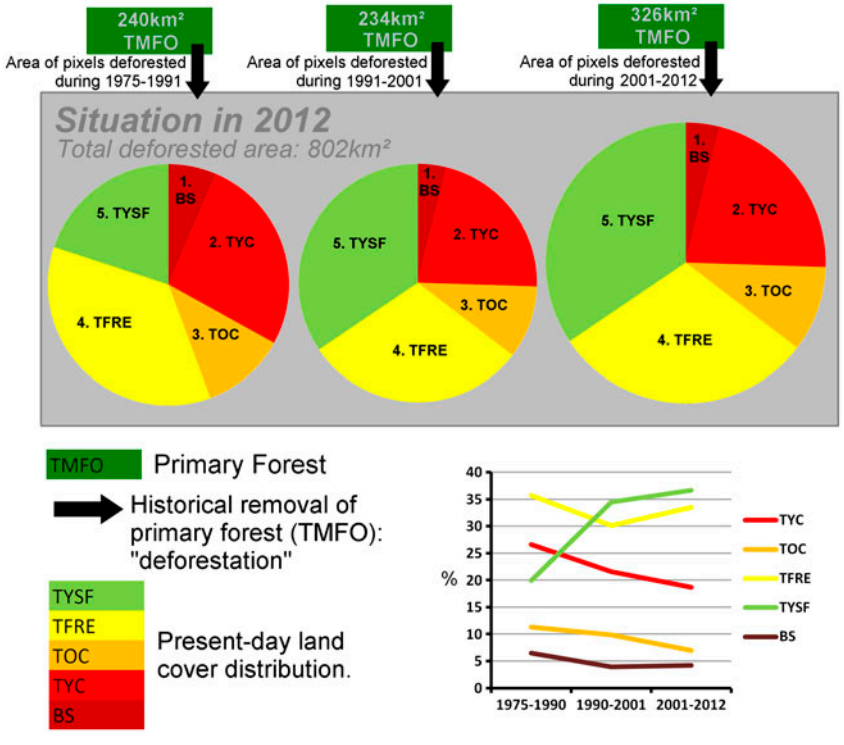

Figure 10. Schematized results. The area of the disks represents the absolute amount of deforested area (km²) during each of the three deforestation periods (Figure 8(a)). Within each of these disks, the different stages of the successional cycle (Figure 6(c)) are indicated in the colored pie charts: the angle of each portion represents the time- and area-normalized proportion of the respective land cover to the total deforested area in that period (%). These areal shares are also shown in the graph (bottom-right).

deforested during 1975–1990. It is likely that this effect will be more pronounced in a few years, as fields deforested during the final years of the 2001–2012 period had not had time to reach the secondary forest stage.

A first explanation is that areas which were deforested longer ago (1975–1990) are often located closer to the village and, due to their proximity, are generally preferred for cultivation (shorter daily walks). Consequently, they are taken back in a next fallow rotation at a younger age, hindering development to mature stages. Second, the capacity of the soil to generate fallow biomass and gain tree dimensions plays a role. The recommended fallow period for a certain production of crops increases with the number of fallow cycles after deforestation (Styger et al., 2007; i.e., time after clearing). In reality, however, the continuous demand for more agricultural land forces more and shorter fallow periods, which causes a fast decline of soil fertility. With advancing soil degradation, regrowth stages require more time to reach mature woody fallow stages (lower growth rates). When the woody stage is not yet reached and the immature fallow is burned once or several times, it may not appear again, leaving a severely degraded soil with impoverished grasslands (Styger et al., 2007), corresponding with a higher share of TYC (Figure 10). Third, some fast-growing species, such as *Musanga cecropiodes* and *Macaranga sp.*, are more abundant on recently cleared primary forest and can very quickly develop typical TYSF characteristics, hence turning the fallow stage of a plot into the TYSF stage. The higher abundance of the above-mentioned species on recently cleared plots can most likely be explained by the gradual depletion of soil seedbanks (Styger et al., 2007) and a decrease in foreign seed rain. Seed rain by animal dispersion (birds and mammals) contributes significantly to establishment of *Musanga* and other forest reconstituting species. The presence of remnant forest trees and less intense human activities were shown to have a positive impact on seed rain in shifting cultivation fields in Cameroon (Carrière, André, Letourmy, Olivier, & McKey, 2002). Both factors are likely to contribute to the slower reconstitution of forest in fields that have undergone several cultivation cycles, as they are generally located closer to villages and further away from primary forest.

For two sub-regions (Figure 3), the same analysis was taken back further in time to the 1959–1975 period (Figure 11(a) and (b)). The most remarkable differences between the deforestation periods, noticed in the overall statistics (cf. the higher TYSF share in recently deforested areas, Figure 10), are still valid for the two subregions. The observed "trends" cannot be extrapolated to the past: the lower share of TYSF does not

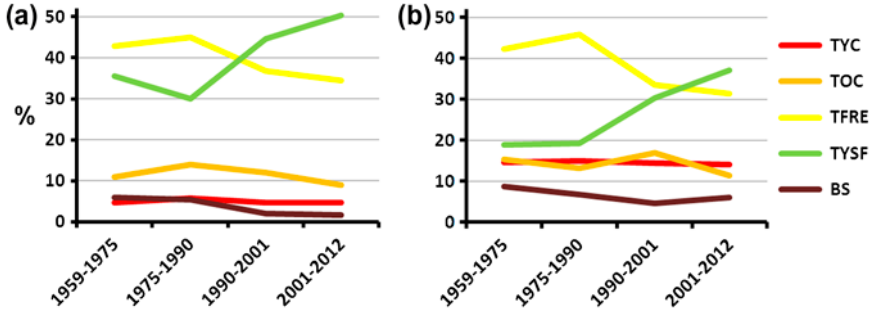

Figure 11. Areal share (%) of individual land-cover classes to deforested area during each period, for sub-regions in (a) the East (left) and (b) West (right).

decrease further with older deforestation age, but stabilizes compared to the level of 1975–1990 (Figure 11(a) and (b)). Areal proportions of the two sub-regions show a similar lower relative abundance of TYSF in areas with older deforestation age (difference of 18–20%).

4.4. *Illustrative application of the main results*

4.4.1. *Validation and completion of gridded reference data-sets*

Our observations in the primary forest were used to validate the values of CH and LAI in the reference data-set of Lawrence and Chase (2007), in which primary forest constitutes one of the PFT's. For CH, the mean observed value is 34.2 m (boxplots in Figure 12 show medians), which is similar to the mean PFT-specific value in the reference data-set of 35 m. Concerning LAI, the mean observed light transmittance is 1.43%, which, after implementation in equation 1 yielded a mean LAI of 5.44 (Figure 12). This is very similar to the mean PFT-specific value (5.43) in the reference data-set. Our (indirectly) measured mean LAI for primary forest is also similar to the mean values found by Wirth et al. (2001) in Panama (5.41), Bohlman, Adams, Smith, and Peterson (1998) in the Amazon (5.3), and De Wasseige and Defourny (2002) in the Central African Republic (5.4). These LAI values exceed typical grid-cell averages for dense forest in the reference data-set (Section 2.2.3) because of averaging over multiple PFT's within the grid cell (which, apart from the 70 to 80% primary forest, also contains non-primary forest PFT's).

Young secondary forest (or *tree fallow*) is not present in the reference data-set of Lawrence and Chase (2007), and hence a validation with observations for the TYSF

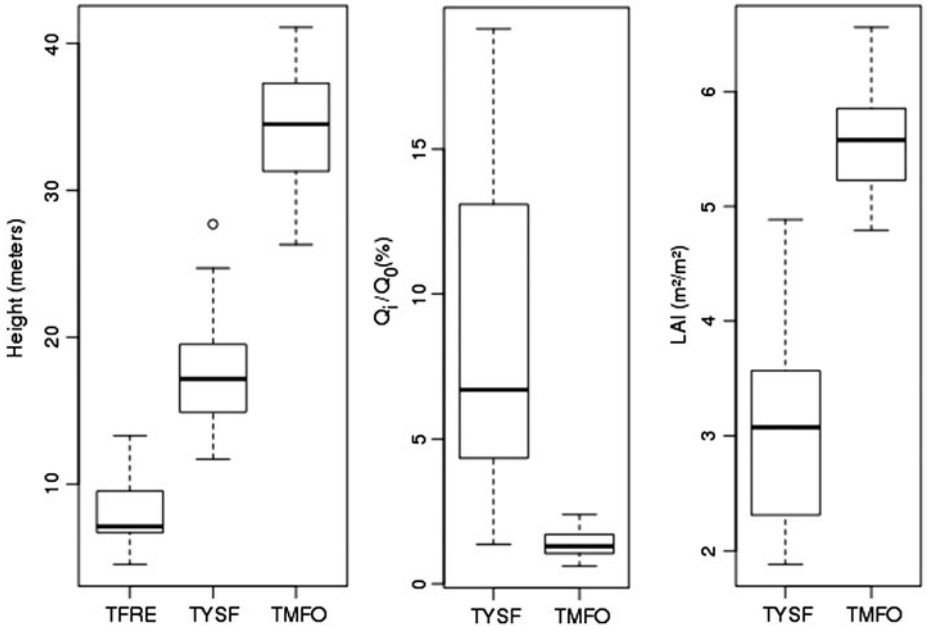

Figure 12. Tree height (left) and canopy light transmittance (center) measured during the field campaign. LAI (right) is derived from light transmittance.

class was not applicable in this case. Mean observed CH (17.5 m), canopy light transmittance (8.15%), and, hence, LAI (2.8 m²/m²) all differ significantly from the values for primary forest (Figure 12). This indicates the important consequences of replacing primary with TYSF, as well as the relative ease of discriminating between the two classes in the field campaign. When relating the observed LAI and CH of secondary forest (TYSF) to primary forest (TMFO), the proportions LAI_{TYSF}/LAI_{TMFO} and CH_{TYSF}/CH_{TMFO} are both about 51%.

4.4.2. *Multiple-class vs. single-class forest conversion*

Future projected CH (CH_{2050}) and LAI (LAI_{2050}) were calculated as area-weighted grid-cell averages (analogous to CH_{2000} and LAI_{2000} in Section 2.2.3), with d being the initially existing areal portion of rainforest in each grid cell (Figure 4(a)), which was replaced by a mix of successional fallow vegetation, and s being a "flag," indicating whether the grid cell was deforested or not (1 or 0) in the scenario:

$$\begin{aligned} LAI_{2050} = d * s * (&0.0487 \cdot LAI_{BS} + 0.2228 \cdot LAI_{TYC} + 0.0938 \cdot LAI_{TOC} \\ &+ 0.3311 \cdot LAI_{TFRE} + 0.3036 \cdot LAI_{TYSF}) + [(1 - d * s) * LAI_{2000}] \end{aligned} \quad (4)$$

CH_{2050} was calculated in a similar way. The factors in Equation 4 are the internal areal proportions as derived from the results of this study. In this way, successional vegetation is implemented in the deforestation scenario with *multiple-class forest conversion.* The resulting gridded field of CH (LAI) is shown in Figure 4(d) and (e). To quantify the difference with *single-class forest conversion*, the scenario was implemented again, but now the deforested portion of the cell was replaced by a single land cover only: crops. The result for CH (LAI) is shown in Figure 4(e) and (f).

Within deforested grid cells, average CH decreased from 25.5 (Figure 4(c)) to 13.36 m when using the deforestation scenario with multiple-class conversion (Figure 4(d)). With the binary forest-to-crops conversion, the mean value would decrease to 7.79 m (Figure 4(e)). As expected, implementing a multiple-class conversion with relative areal proportions from our study resulted in less drastic but more realistic projections. When considering LAI, the difference between both approaches was less distinct, as the average value of 4.3 within deforested grid cells decreased to 2.86 with the *multiple-class conversion* and to 2.63 with the *single-class conversion.*

5. Discussion

These findings could have serious consequences for impact studies, such as those investigating the change of carbon stocks associated with deforestation and regeneration. Assuming a linear relation between tree height and carbon stock (which is of course a very simplified and carbon-overestimating model), the use of this deforestation scenario with a *single-class* conversion method would overestimate the decrease in carbon stocks by 46% compared to a scenario complemented with a *multiple-class* conversion. In more complex models, such as state-of-the-art regional climate models, the difference of using a deforestation scenario with *single-class* or with *multiple-class* forest conversion could result in profoundly different energy fluxes and exchanges of water between the earth surface and the atmosphere. Consequently, these studies would probably find a more realistic impact of forest removal on the regional climate.

This study only discusses a small part of the Congo Basin rainforest and is therefore not representative for global tropical deforestation land-cover sequences. It is rather meant to show the potential of GIS studies to complement (or refine) the existing relatively simple (binary) deforestation scenarios with multiple-class forest conversion in their use for environmental and climatological modeling studies.

6. Summary and conclusions

This study sought to identify the present-day successional land-cover types along the forest frontier in the Congo Basin and quantify their areal proportions. An additional aim was to investigate the dependency of these proportions on time since deforestation. A multi-temporal GIS approach was followed, allowing the categorization of the total deforested region in three, near-decadal, deforestation periods.

Primary forest in all images was detected using an unsupervised identification algorithm, resulting in four maps with primary forest vs. remainder (1975, 1990, 2001, and 2012), and consequently subtracted to calculate three periodic forest change maps (1975–1990, 1990–2001 and 2001–2012). In addition, the present-day image (2012) was classified in five successional land-cover classes with a supervised classification technique. The supervised classification was undertaken with *a priori* defined successional vegetation stages as land-cover classes, and the resulting land-cover map was validated. Overall, the classification performance was satisfactory.

For each of the three deforestation periods, the corresponding grid cells in the present-day land-cover map were extracted and analyzed; this resulted in a certain relative areal proportion of current land cover for each deforestation period. When the relation between present-day land cover and deforestation age was analyzed, some significant differences became visible: especially, the present-day areal proportion of TYSF was found to be lower in regions deforested more than 20 years ago. Possible reasons for this are the preference to cultivate in nearby areas, resulting in fewer fallow sites reaching the TYSF stage, and soil over-exploitation, resulting in degradation of the vegetative composition. Furthermore, a changing species composition (with a decrease of fast-growing species abundance) could be an important contributing factor.

The main results of this study consist of the long-term average areal proportions of successional vegetation (over the three deforestation periods in the larger study area) being 4.9% BS, 22.3% TYC, 9.4% TOC, 33.1% TFRE, and 30.7% TYSF. In an illustrative application, we refined the future deforestation projection of Zhang et al. (2006) using these results in a multiple-class forest conversion and created maps of projected CH for 2050. Mean CH was overestimated by 46% when using *single-class* compared to a *multiple-class* forest conversion. This indicates that the methodology we proposed for refining existing deforestation scenarios is important for impact-modeling studies, in which the uncertainty is often related to the implemented deforestation scenarios.

Acknowledgements

This research was made possible through the support of VLIR-UOS for both a PhD fellowship for Pieter Moonen and the Congo project DEFI (Développement Economique des Forêts à travers une utilization Informée) for the fieldwork. The authors thank the University of Kisangani for the support during the field campaign. The authors sincerely appreciate the efforts of two anonymous reviewers in improving this manuscript.

References

Ball, G. H., & Hall, D. J. (1965). *ISODATA a novel method of data analysis and pattern classification* (Technical Report). Stanford, CA: Stanford University.

Bamba, I., Barima, Y. S. S., & Bogaert, J. (2010). Influence de la densité de la population sur la structure spatiale d'un paysage forestier dans le bassin du Congo en RD Congo [Influence of population density on the spatial structure of a forest landscape in the Congo Basin in DR Congo]. *Mongabay.com Open Access Journal – Tropical Conservation Science, 3*, 31–44.

Bazzaz, F., & Pickett, S. (1980). Physiological ecology of tropical succession: A comparative review. *Annual Review of Ecology and Systematics, 11*, 287–310.

Bohlman, S. A., Adams, J. B., Smith, M. O., & Peterson, D. L. (1998). Seasonal foliage changes in the eastern Amazon basin detected from Landsat Thematic Mapper satellite images. *Biotropica*, *30*, 376–391.

Bruce, C. M., & Hilbert, D. W. (2006). *Pre-processing methodology for application to Landsat TM/ETM + Imagery of the wet tropics*. Cooperative Research Centre for Tropical Rainforest Ecology and Management. Cairns: Rainforest CRC.

Butler, R. A., & Laurance, W. F. (2008). New strategies for conserving tropical forests. *Trends in Ecology & Evolution*, *23*, 469–472.

Carrière, S. M., André, M., Letourmy, P., Olivier, I., & McKey, D. B. (2002). Seed rain beneath remnant trees in a slash-and-burn agricultural system in southern Cameroon. *Journal of Tropical Ecology*, *18*, 353–374.

Cournac, L., Dubois, M.-A., Chave, J., & Riéra, B. (2002). Fast determination of light availability and leaf area index in tropical forests. *Journal of Tropical Ecology*, *18*, 295–302.

De Wasseige, C., & Defourny, P. (2002). Retrieval of tropical forest structure characteristics from bi-directional reflectance of SPOT images. *Remote Sensing of Environment*, *83*, 362–375.

Defries, R. S., Bounoua, L., & Collatz, G. J. (2002). Human modification of the landscape and surface climate in the next fifty years. *Global Change Biology*, *8*, 438–458.

Dobois, J. C. L. (1996). Forest-dependent people. *Unasylva*, *47*(186). Retrieved from http://www.fao.org/docrep/w1033e/w1033e04.htm

Emmons, L., Chatelet, P., Cournac, L., Pitman, N. C. A., Vilca, V. V., Fernando Del Aguila, L. F., & Dubois, M. A. (2006). Seasonal change in leaf-area index at three sites along a South American latitudinal gradient. *Ecotropica*, *12*, 87–102.

FACET. (2010). *Monitoring the forests of Central Africa using remotely sensed data sets (FACET) Forest cover and forest cover loss in the Democratic Republic of Congo from 2000 to 2010*. Brookings: South Dakota State University.

Feddema, J. J., Oleson, K. W., Bonan, G. B., Mearns, L. O., Buja, L. E., Meehl, G. A., & Washington, W. M. (2005). The importance of land-cover change in simulating future climates. *Science*, *310*, 1674–1678.

Kitajima, K., Mulkey, S. S., & Wright, S. J. (2005). Variation in crown light utilization characteristics among tropical canopy trees. *Annals of Botany*, *95*, 535–547.

Lawrence, P. J., & Chase, T. N. (2007). Representing a new MODIS consistent land surface in the Community Land Model (CLM 3.0). *Journal of Geophysical Research*, *112*(G1), 1–17.

Lebamba, J., Ngomanda, A., Vincens, A., Jolly, D., Favier, C., Elenga, H., & Bentaleb, I. (2009). Central African biomes and forest succession stages derived from modern pollen data and plant functional types. *Climate of the Past*, *5*, 403–429.

Makana, J.-R., & Thomas, S. C. (2006). Impacts of selective logging and agricultural clearing on forest structure floristic composition and diversity and timber tree regeneration in the Ituri Forest Democratic Republic of Congo. *Biodiversity and Conservation*, *15*, 1375–1397.

Mayaux, P., De Grandi, G., & Malingreau, J.-P. (2000). Central African forest cover revisited. *Remote Sensing of Environment*, *71*, 183–196.

Maynard, K., & Royer, J.-F. (2004). Effects of "realistic" land-cover change on a greenhouse-warmed African climate. *Climate Dynamics*, *22*, 343–358.

Norris, K., Asase, A., Collen, B., Gockowksi, J., Mason, J., Phalan, B., & Wade, A. (2010). Biodiversity in a forest-agriculture mosaic – The changing face of West African rainforests. *Biological Conservation*, *143*, 2341–2350.

Oleson, K. W., Lawrence, D. M., Flanner, M. G., Kluzek, E. J. P., Levis, S., Swenson, S. C., … Zeng, X. (2010). *Technical description of version 4.0 of the Community Land Model (CLM)*. Boulder, CO: National Center for Atmospheric Research (NCAR).

Ortiz, M. J., Formaggio, A. R., & Epiphanio, J. C. N. (1997). Classification of croplands through integration of remote sensing GIS and historical database. *International Journal of Remote Sensing*, *18*, 95–105.

Polcher, J., & Laval, K. (1994). The impact of African and Amazonian deforestation on tropical climate. *Journal of Hydrology*, *155*, 389–405.

Richards, J. A. (1999). *Remote sensing digital image analysis* (p. 240). Berlin: Springer-Verlag.

Russell, D., Mbile, P., & Tchamou, N. (2011). Farm and forest in Central Africa: Toward an integrated rural development strategy. *Journal of Sustainable Forestry*, *30*, 111–132.

Semazzi, F. H., & Song, Y. (2001). A GCM study of climate change induced by deforestation in Africa. *Climate Research*, *17*, 169–182.

Song, C., Woodcock, C. E., Seto, K. C., Lenney, M. P., & Macomber, S. A. (2001). Classification and change detection using Landsat TM data: When and how to correct atmospheric effects? *Remote Sensing of Environment*, *75*, 230–244.

Strengers, B., Leemans, R., Eickhout, B., Vries, B., & Bouwman, L. (2004). The land-use projections and resulting emissions in the IPCC SRES scenarios scenarios as simulated by the IMAGE 2.2 model. *GeoJournal*, *61*, 381–393.

Styger, E., Rakotondramasy, H. M., Pfeffer, M. J., Fernandes, E. C. M., & Bates, D. M. (2007). Influence of slash-and-burn farming practices on fallow succession and land degradation in the rainforest region of Madagascar. *Agriculture Ecosystems & Environment*, *119*, 257–269.

Sud, Y. C., Lau, W. K.-M., Walker, G. K., Kim, J.-H., Liston, G. E., & Sellers, P. J. (1996). Biogeophysical consequences of a tropical deforestation scenario: A GCM simulation study. *Journal of Climate*, *9*, 3225–3247.

Van Vliet, N., Mertz, O., Heinimann, A., Langanke, T., Pascual, U., Schmook, B., … Ziegler, A. D. (2012). Trends drivers and impacts of changes in swidden cultivation in tropical forest-agriculture frontiers: A global assessment. *Global Environmental Change*, *22*, 418–429.

Vancutsem, C., Pekel, J.-F., Evrard, C., Malaisse, F., & Defourny, P. (2009). Mapping and characterizing the vegetation types of the Democratic Republic of Congo using SPOT VEGETATION time series. *International Journal of Applied Earth Observation and Geoinformation*, *11*, 62–76.

Wirth, R., Weber, B., & Ryel, R. J. (2001). Spatial and temporal variability of canopy structure in a tropical moist forest. *Acta Oecologica*, *22*, 235–244.

Zhang, Q., Justice, C. O., Jiang, M., Brunner, J., & Wilkie, D. S. (2006). A GIS-based assessment on the vulnerability and future extent of the tropical forests of the Congo Basin. *Environmental Monitoring and Assessment*, *114*, 107–121.